Spectral Analysis of a New Six-Phase Pole-Changing Induction Motor Drive for Electric Vehicles

S. Z. Jiang, K. T. Chau, *Member, IEEE*, and C. C. Chan, *Fellow, IEEE*

***Abstract*—In this paper, a new six-phase pole-changing induction motor drive is proposed to extend the constant-power operating range for electric vehicle application. The double Fourier series is newly employed to analyze the spectra of the motor phase voltage and current. Consequently, the harmonic expression of the inverter dc-link current can be derived. In order to reduce the dc-link harmonics, a new sinusoidal pulsewidth-modulation strategy is developed for the proposed six-phase inverter. Experimental results, particularly the spectra of the phase current and the dc-link current, are given to verify the theoretical analysis.**

***Index Terms*—Electric vehicles (EVs), induction motor drives, pole changing, spectral analysis.**

I. Introduction

THE squirrel-cage induction motor (SCIM) has been identified as being one of the most viable motors for modern electric vehicles (EVs) [1]. Nevertheless, there is still one obstacle for its wide application to EV propulsion, namely, the difficulty in providing constant-power operation for the high-speed range of EVs. Thus, the inverter-fed six-phase pole-changing SCIM drive is becoming attractive for modern EVs [2].

Recently, a new six-phase pole-changing SCIM drive has been fproposed for EVs [3]. Both the maximum torque characteristics and harmonic torque have been analyzed by circuit simulation, indicating its promising application to EV propulsion. However, the circuit simulation cannot give an insight into the spectrum of the phase current and, hence, that of the dc-link current. It should be noted that the dc-link harmonic currents cause the rise of the battery temperature and, consequently, decrease the battery lifetime. The battery lifetime is the most important factor to affect the operating cost of EVs [4].

For three-phase inverters, there are many pulsewidth-modulation (PWM) schemes that have been developed to reduce the output harmonics and, hence, the dc-link harmonics [5]. Nevertheless, the six-phase inverter provides the feasibility to further reduce the harmonic content of the dc link. In [6], a dual inverter, the so-called the double-pulse inverter, was used to feed a six-phase SCIM. It proposed to shift the phase between two carriers of the dual inverter so as to reduce the dc-link harmonics. However, the corresponding analysis was essentially qualitative and no experimental verification for the harmonic reduction was given.

Manuscript received June 4, 2001; revised May 12, 2002. Abstract published on the Internet November 20, 2002. This work was supported in part by an RGC research grant from the Hong Kong Research Grants Council and a CRCG research grant from the University of Hong Kong.

The authors are with the Department of Electrical and Electronic Engineering, University of Hong Kong, Hong Kong (e-mail: ktchau@eee.hku.hk).

Digital Object Identifier 10.1109/TIE.2002.807662

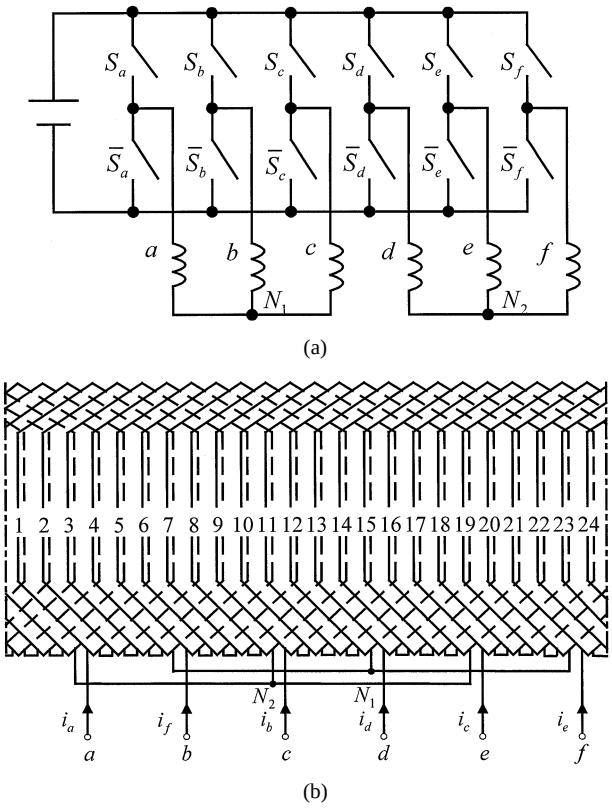

Fig. 1. Inverter-fed six-phase pole-changing SCIM drive. (a) Six-phase inverter. (b) Six-phase winding connections.

The purpose of this paper is to develop a new inverter-fed six-phase pole-changing SCIM drive for EV propulsion, with emphasis on the spectral analysis of the motor phase current and the inverter dc-link current. Both phase shifts between two references and between two carriers of the six-phase PWM inverter will be proposed to achieve electronic pole changing and harmonic suppression, respectively. In order to analytically assess the dc-link harmonics, the double Fourier series will be employed. Finally, experimental results will be given to verify the theoretical analysis.

II. Pole-Changing SCIM Drive

Fig. 1 shows the proposed inverter-fed six-phase pole-changing SCIM drive. The key is to split the conventional three-phase windings A-B-C into two sets of three-phase windings a-b-c and d-e-f, the so-called dual-star six-phase windings. There are 24 slots in the stator of the designed motor. All 24 coils are of double layers. The corresponding winding connection is illustrated in Fig. 1(b).

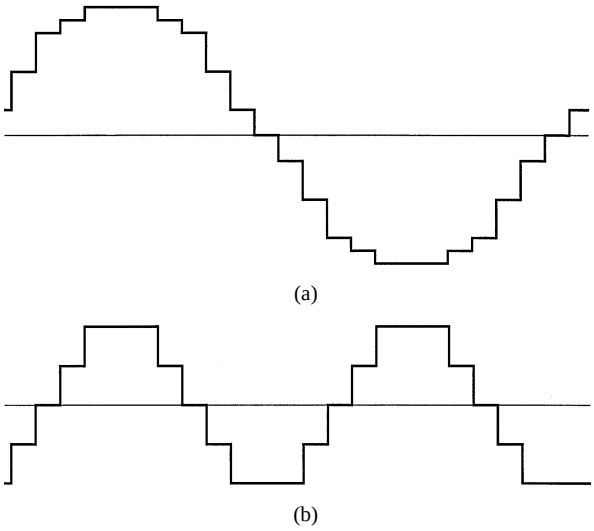

Fig. 2. Pole-changing MMF waveforms. (a) Two-pole. (b) Four-pole.

Fig. 2 shows the magnetomotive force (MMF) waveforms at the instant that the current of the phase-a winding reaches its maximum value. In Fig. 2(a), the currents of two star-connected windings are out of phase, producing the two-pole MMF waveform. In Fig. 2(b), the two currents become in phase, producing the four-pole MMF waveform. Thus, the number of poles can be altered by changing the phase difference between the currents of two star-connected windings. Hence, by controlling the switching signals of the inverter for this six-phase SCIM, the corresponding pole pairs can be changed electronically.

III. Six-Phase Inverter Operation

The proposed six-phase inverter is considered as two three-phase inverters operating simultaneously. In both three-phase inverters, the natural sampled PWM algorithm is adopted, where the switching signals are generated by comparing a sinusoidal reference with a triangular carrier, as shown in Fig. 3(a). For four-pole operation, the phases and amplitudes of the two sets of three-phase references are identical. Under this condition, the phase difference between two triangular carriers leads to two possible cases on how to generate the PWM signals—namely, the case 4P1 in which the two carriers are in phase, and the case 4P2 in which the two carriers are exactly out of phase. On the other hand, for two-pole operation, the phases of the two sets of three-phase references are exactly out of phase while their amplitudes are kept the same. Correspondingly, there are also two possible cases—2P1 and 2P2 in which the phase differences between two carriers are in phase and exactly out of phase, respectively.

In order to identify the appropriate cases for the proposed six-phase inverter, spectral analysis of the corresponding harmonic distributions is conducted by means of the double Fourier series [7]. To simplify the analysis, some basic assumptions are made: the power devices are ideal, the dead time is negligible, and the dc-link voltage is constant. The phase-a voltage with respect to the negative terminal of the dc link, u_{ao}, is adopted for exemplification. Based on $\alpha = \omega_r t$ and $\beta = \omega_c t$ (ω_r is the angular frequency of the reference and ω_c is the angular frequency of the carrier), the time axis shown in Fig. 3(a) can be

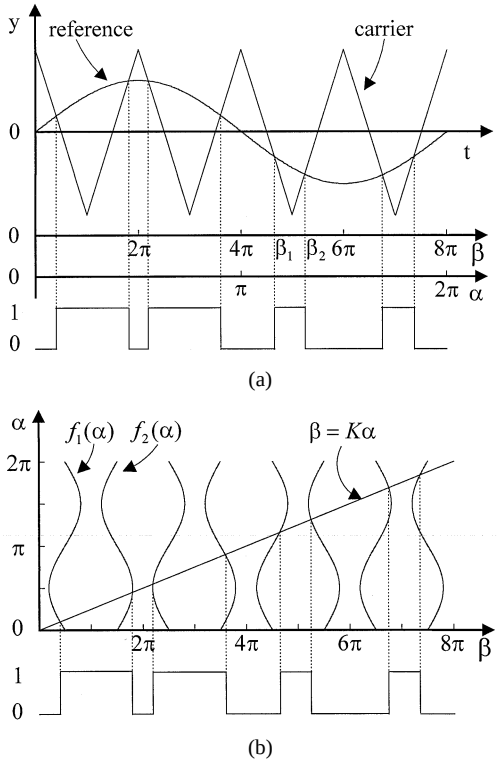

Fig. 3. Representations of PWM signal generation. (a) Time-domain representation. (b) Angular-domain representation.

transformed to two angular axes α and β. The triangular carrier and sinusoidal reference are then, respectively, represented by

$$y = \begin{cases} -\frac{2}{\pi}\beta + 1 & 2n\pi \le \beta \le (2n+1)\pi, \\ \frac{2}{\pi}\beta - 3 & (2n+1)\pi \le \beta \le (2n+2)\pi \end{cases}, \quad n = 0, 1, 2, \ldots \tag{1}$$

$$y = M \sin\alpha \tag{2}$$

where M is the modulation index. By solving (1) and (2), the intersection abscissas on the axis within a carrier cycle are given by

$$\beta_1 = \frac{\pi}{2}(1 - M\sin\alpha), \quad \frac{2n\pi}{K} \le \alpha \le \frac{(2n+1)\pi}{K} \tag{3}$$

$$\beta_2 = 2\pi - \frac{\pi}{2}(1 - M\sin\alpha), \quad \frac{(2n+1)\pi}{K} \le \alpha \le \frac{(2n+2)\pi}{K} \tag{4}$$

where $n = 0, 1, 2 \ldots, K-1$, and K is the modulation ratio defined as ω_c/ω_r.

On the $\alpha-\beta$ plane, the angular representation of PWM signal generation is illustrated in Fig. 3(b). Within each 2π period, the intersection abscissas between the line $\beta = K\alpha$ and the sinusoidal curves $f_1(\alpha) = (\pi/2)(1 - M\sin\alpha)$ and $f_2(\alpha) = 2\pi - (\pi/2)(1 - M\sin\alpha)$ satisfy (3) and (4). If K is an integer, the resulted PWM signal is repetitive over each $2K\pi$ along the β axis and over each 2π along the α axis. Thus, the two representations in Fig. 3 are equivalent. Consequently, the PWM voltage u_{ao} can be defined as

$$u_{ao}(\alpha,\beta) = \begin{cases} 0, & 0 \le \beta \le f_1(\alpha) \\ V_d, & f_1(\alpha) \le \beta \le f_2(\alpha) \\ 0, & f_2(\alpha) \le \beta \le 2\pi \end{cases} \tag{5}$$

where V_d is the dc-link voltage, and $u_{ao}(\alpha,\beta)$ is a periodic function. By applying the double Fourier series, it can be expressed as

$$\begin{aligned} u_{ao}(\alpha,\beta) =& \frac{1}{2}A_{00} + B_{01}\sin\alpha \\ &+ \sum_{i=1,3,5}^{\infty}\sum_{j=0,\pm2,\pm4}^{\pm\infty} A_{ij}\cos(i\beta + j\alpha) \\ &+ \sum_{i=2,4,6}^{\infty}\sum_{j=\pm1,\pm3,\pm5}^{\pm\infty} B_{ij}\sin(i\beta + j\alpha) \end{aligned} \quad (6)$$

where $A_{00} = V_d$, $B_{01} = MV_d/2$, $A_{ij} = (-1)^{(i+1/2)}(2V_d/i\pi)J_j(i\pi M/2)$, and $B_{ij} = (-1)^{i/2}(2V_d/i\pi)J_j(i\pi M/2)$. Notice that J_i is the Bessel function of the first kind defined as $J_j(\zeta) = (1/2\pi)\int_0^{2\pi}\cos(\zeta\sin(x) - jx)dx$.

With the transformations of $\alpha = \omega_r t$ and $\beta = \omega_c t$, (6) is rewritten as

$$\begin{aligned} u_{ao}(\omega_r t,\omega_c t) =& \frac{1}{2}A_{00} + B_{01}\sin\omega_r t \\ &+ \sum_{i=1,3,5}^{\infty}\sum_{j=0,\pm2,\pm4}^{\pm\infty} A_{ij} \\ &\times \cos(i\omega_c t + j\omega_r t) \\ &+ \sum_{i=2,4,6}^{\infty}\sum_{j=\pm1,\pm3,\pm5}^{\pm\infty} B_{ij} \\ &\times \sin(i\omega_c t + j\omega_r t). \end{aligned} \quad (7)$$

Hence, the phase b voltage with respect to the negative terminal of the dc link, u_{bo}, can be deduced as

$$\begin{aligned} u_{bo}(\omega_r t,\omega_c t) =& \frac{1}{2}A_{00} + B_{01}\sin\left(\omega_r t - \frac{2\pi}{3}\right) \\ &+ \sum_{i=1,3,5}^{\infty}\sum_{j=0,\pm2,\pm4}^{\pm\infty} A_{ij} \\ &\times \cos\left\{i\omega_c t + j\left(\omega_r t - \frac{2\pi}{3}\right)\right\} \\ &+ \sum_{i=2,4,6}^{\infty}\sum_{j=\pm1,\pm3,\pm5}^{\pm\infty} B_{ij} \\ &\times \sin\left\{i\omega_c t + j\left(\omega_r t - \frac{2\pi}{3}\right)\right\}. \end{aligned} \quad (8)$$

Subtracting (8) from (7), the line voltage between phases a and b is given by

$$\begin{aligned} u_{ab}(\omega_r t,\omega_c t) =& u_{ao}(\omega_r t,\omega_c t) - u_{bo}(\omega_r t,\omega_c t) \\ =& \sqrt{3}B_{01}\sin\left(\omega_r t + \frac{\pi}{6}\right) \\ &+ \sum_{i=1,3,5}^{\infty}\sum_{j=0,\pm2,\pm4}^{\pm\infty} \sqrt{3}A_{ij} \\ &\times \cos\left\{i\omega_c t + j\left(\omega_r t + \frac{\pi}{6}\right)\right\} \\ &+ \sum_{i=2,4,6}^{\infty}\sum_{j=\pm1,\pm3,\pm5}^{\pm\infty} \sqrt{3}B_{ij} \\ &\times \sin\left\{i\omega_c t + j\left(\omega_r t + \frac{\pi}{6}\right)\right\}. \end{aligned} \quad (9)$$

TABLE I
DOUBLE FOURIER SERIES OF PHASE-d VOLTAGE

Cases	References	Carriers	$\sin\omega_r t$	$\cos(i\omega_c t + j\omega_r t)$	$\sin(i\omega_c t + j\omega_r t)$
4P1	0°	0°	B_{01}	A_{ij}	B_{ij}
4P2	0°	180°	B_{01}	$-A_{ij}$	B_{ij}
2P1	180°	0°	$-B_{01}$	A_{ij}	$-B_{ij}$
2P2	180°	180°	$-B_{01}$	$-A_{ij}$	$-B_{ij}$

As a result, the phase voltage of phase a can be obtained as

$$\begin{aligned} u_a(\omega_r t,\omega_c t) =& B_{01}\sin\omega_r t \\ &+ \sum_{i=1,3,5}^{\infty}\sum_{j=0,\pm2,\pm4}^{\pm\infty} A_{ij}\cos(i\omega_c t + j\omega_r t) \\ &+ \sum_{i=2,4,6}^{\infty}\sum_{j=\pm1,\pm3,\pm5}^{\pm\infty} B_{ij} \\ &\times \sin(i\omega_c t + j\omega_r t). \end{aligned} \quad (10)$$

Based on the phase relations between phases a and d for the four cases, the double Fourier series of the phase d voltage u_d can readily be deduced from (10). In the case 4P1, there are no phase differences between the two references and between the two carriers, the phase d voltage is identical to the phase a voltage. In the case 4P2, due to the phase differences of 180° between the two carriers, the second term of becomes out of phase with respect to that in (10). For the case 2P1, due to the phase difference of 180° between the two references, the first and the third terms become out of phase. For the case 2P2, since both the two references and the two carriers are out of phase, all the three terms are out of phase. Under the same battery voltage and modulation index, Table I summarizes the double Fourier series coefficients of the phase d voltage in all four cases.

From (10), it can be found that the phase voltage includes two parts: the first term is the reference-frequency component, the second and the third terms are the cross-modulation components. When the modulation ratio K is an even number, the second term represents the even harmonics, and the third term denotes the odd harmonics. Hence, both odd and even harmonics are present in the phase voltage. When K is an odd number, both the second and the third terms are odd harmonics, leading to the presence of odd harmonics only in the phase voltage. Therefore, an odd modulation ratio is purposely adopted to eliminate the even harmonics.

When the magnetic saturation effect of the SCIM is neglected, the fundamental and harmonic phase voltages can be regarded as independent voltage sources. The fundamental and harmonic currents can then be calculated by using the per phase equivalent circuit shown in Fig. 4. The corresponding parameter values measured at 50 Hz are also listed with and without brackets for two-pole and four-pole operation, respectively. In the star-connected windings, the triplen harmonic voltages cannot produce the corresponding harmonic currents. From (10), the current of phase a in four possible cases can be

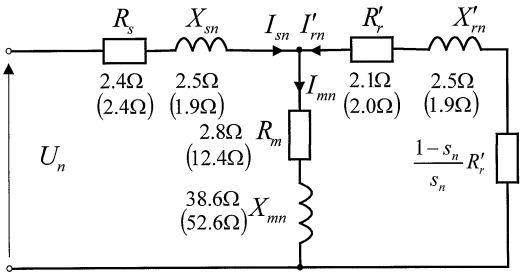

Fig. 4. Pre-phase equivalent circuit.

expressed as

$$\begin{aligned} i_a(\omega_r t,\omega_c t) =& \frac{B_{01}}{|Z_1|}\sin(\omega_r t-\varphi_1) \\ &+\sum_{i=1,3,5}^{\infty}\sum_{\substack{j=0,\pm2,\pm4\\ iK+j\neq 3h}}^{\pm\infty}\frac{A_{ij}}{|Z_{A,ij}|} \\ &\times\cos(i\omega_c t+j\omega_r t-\varphi_{A,ij}) \\ &+\sum_{i=2,4,6}^{\infty}\sum_{\substack{j=\pm1,\pm3,\pm5\\ iK+j\neq 3h}}^{\pm\infty}\frac{B_{ij}}{|Z_{B,ij}|} \\ &\times\sin(i\omega_c t+j\omega_r t-\varphi_{B,ij}) \end{aligned} \tag{11}$$

where h is a positive integer, Z_1, $Z_{A,ij}$, and $Z_{B,ij}$ are the equivalent input impedances, and φ_1, $\varphi_{A,ij}$ and $\varphi_{B,ij}$ are their phase angles. Hence, the current of phase d in the cases 4P1 and 4P2 can be obtained as

$$\begin{aligned} i_d(\omega_r t,\omega_c t) =& \frac{B_{01}}{|Z_1|}\sin(\omega_r t-\varphi_1) \\ &\pm\sum_{i=1,3,5}^{\infty}\sum_{\substack{j=0,\pm2,\pm4\\ iK+j\neq 3h}}^{\pm\infty}\frac{A_{ij}}{|Z_{A,ij}|} \\ &\times\cos(i\omega_c t+j\omega_r t-\varphi_{A,ij}) \\ &+\sum_{i=2,4,6}^{\infty}\sum_{\substack{j=\pm1,\pm3,\pm5\\ iK+j\neq 3h}}^{\pm\infty}\frac{B_{ij}}{|Z_{B,ij}|} \\ &\times\sin(i\omega_c t+j\omega_r t-\varphi_{B,ij}) \end{aligned} \tag{12}$$

where the "+" sign is for the case 4P1 and the "−" sign is for the case 4P2. Similarly, the current of phase d in the cases 2P1 and 2P2 can be obtained as

$$\begin{aligned} i_d(\omega_r t,\omega_c t) =& -\frac{B_{01}}{|Z_1|}\sin(\omega_r t-\varphi_1) \\ &\pm\sum_{i=1,3,5}^{\infty}\sum_{\substack{j=0,\pm2,\pm4\\ iK+j\neq 3h}}^{\pm\infty}\frac{A_{ij}}{|Z_{A,ij}|} \\ &\times\cos(i\omega_c t+j\omega_r t-\varphi_{A,ij}) \\ &-\sum_{i=2,4,6}^{\infty}\sum_{\substack{j=\pm1,\pm3,\pm5\\ iK+j\neq 3h}}^{\pm\infty}\frac{B_{ij}}{|Z_{B,ij}|} \\ &\times\sin(i\omega_c t+j\omega_r t-\varphi_{B,ij}) \end{aligned} \tag{13}$$

where the "+" sign is for the case 2P1 and the "−" sign is for the case 2P2.

Due to the symmetry property, the currents of other phases can be easily derived from (11)–(13). By selecting $M=0.8$, $K=45$, $V_d=110$ V and using (11)–(13), the simulated current waveforms of both phases a and d at the synchronous speed of 1500 r/min and the load of 150 W are shown in Fig. 5. They testify that the fundamental currents, hence, the number of pole pairs, are only dependent on the phase between references, and are irrelevant to the phase between carriers. In the four possible cases, the phase currents have a similar spectral pattern. The spectrum of phase a current is illustrated in Fig. 6. It can be observed that the larger harmonic amplitudes concentrate nearby the multiples of the carrier frequency. Their order numbers are $mK\pm n$, where m and n are not simultaneously even or odd.

IV. Harmonics of DC Link

Since the power devices of the six-phase inverter are assumed to be ideal, the instantaneous power absorbed by the motor is equal to that supplied by the battery. This yields

$$i=\frac{u_a i_a+u_b i_b+u_c i_c}{V_d}+\frac{u_d i_d+u_e i_e+u_f i_f}{V_d} \tag{14}$$

where i is the dc-link current, u_a, u_b, u_c, u_d, u_e, and u_f are the phase voltages, and i_a, i_b, i_c, i_d, i_e, and i_f are the phase currents. It can be found that the first part in (14) is contributed to by the voltages and currents of the windings a, b and c. It can be expressed as

$$\frac{u_a i_a+u_b i_b+u_c i_c}{V_d}=i_{abc,\mathrm{DC}}+i_{abc,\mathrm{even}}+i_{abc,\mathrm{odd}}. \tag{15}$$

For four-pole operation, by using (10)–(12), the three terms in (15) can be written as

$$\begin{aligned} i_{abc,\mathrm{DC}} =& \frac{3B_{01}^2}{2V_d|Z_1|}\cos\varphi_1 \\ &+\frac{3}{2V_d}\sum_{i=1,3,5}^{\infty}\sum_{\substack{j=0,\pm2,\pm4\\ iK+j\neq 3h}}^{\pm\infty}\frac{A_{ij}^2}{|Z_{A,ij}|}\cos\varphi_{A,ij} \\ &+\frac{3}{2V_d}\sum_{i=2,4,6}^{\infty}\sum_{\substack{j=\pm1,\pm3,\pm5\\ iK+j\neq 3h}}^{\pm\infty}\frac{B_{ij}^2}{|Z_{B,ij}|}\sin\varphi_{B,ij} \end{aligned} \tag{16}$$

$$\begin{aligned} i_{abc,\mathrm{even}} =& \frac{3B_{01}}{2V_d}\sum_{\substack{i=2,4,6\\ iK+j\neq 3h}}^{\infty}\sum_{\substack{l=0,\pm1,\pm2\\ j=6l-5}}^{\pm\infty}\frac{B_{ij}}{|Z_{B,ij}|} \\ &\times\cos[i\omega_c t+(j-1)\omega_r t-\varphi_{B,ij}] \\ &-\frac{3B_{01}}{2V_d}\sum_{\substack{i=2,4,6\\ iK+j\neq 3h}}^{\infty}\sum_{\substack{l=0,\pm1,\pm2\\ j=6l-1}}^{\pm\infty}\frac{B_{ij}}{|Z_{B,ij}|} \\ &\times\cos[i\omega_c t+(j+1)\omega_r t-\varphi_{B,ij}] \\ &+\frac{3B_{01}}{2V_d|Z_1|}\sum_{i=2,4,6}^{\infty}\sum_{\substack{l=0,\pm1,\pm2\\ j=6l-5}}^{\pm\infty}B_{ij} \\ &\times\cos[i\omega_c t+(j-1)\omega_r t+\varphi_1] \\ &-\frac{3B_{01}}{2V_d|Z_1|}\sum_{i=2,4,6}^{\infty}\sum_{\substack{l=0,\pm1,\pm2\\ j=6l-1}}^{\pm\infty}B_{ij} \\ &\times\cos[i\omega_c t+(j+1)\omega_r t-\varphi_1] \\ &+i_{a,\mathrm{even}}(\omega_c t,\omega_r t)+i_{a,\mathrm{even}}\left(\omega_c t,\omega_r t-\frac{2\pi}{3}\right) \\ &+i_{a,\mathrm{even}}\left(\omega_c t,\omega_r t+\frac{2\pi}{3}\right) \end{aligned} \tag{17}$$

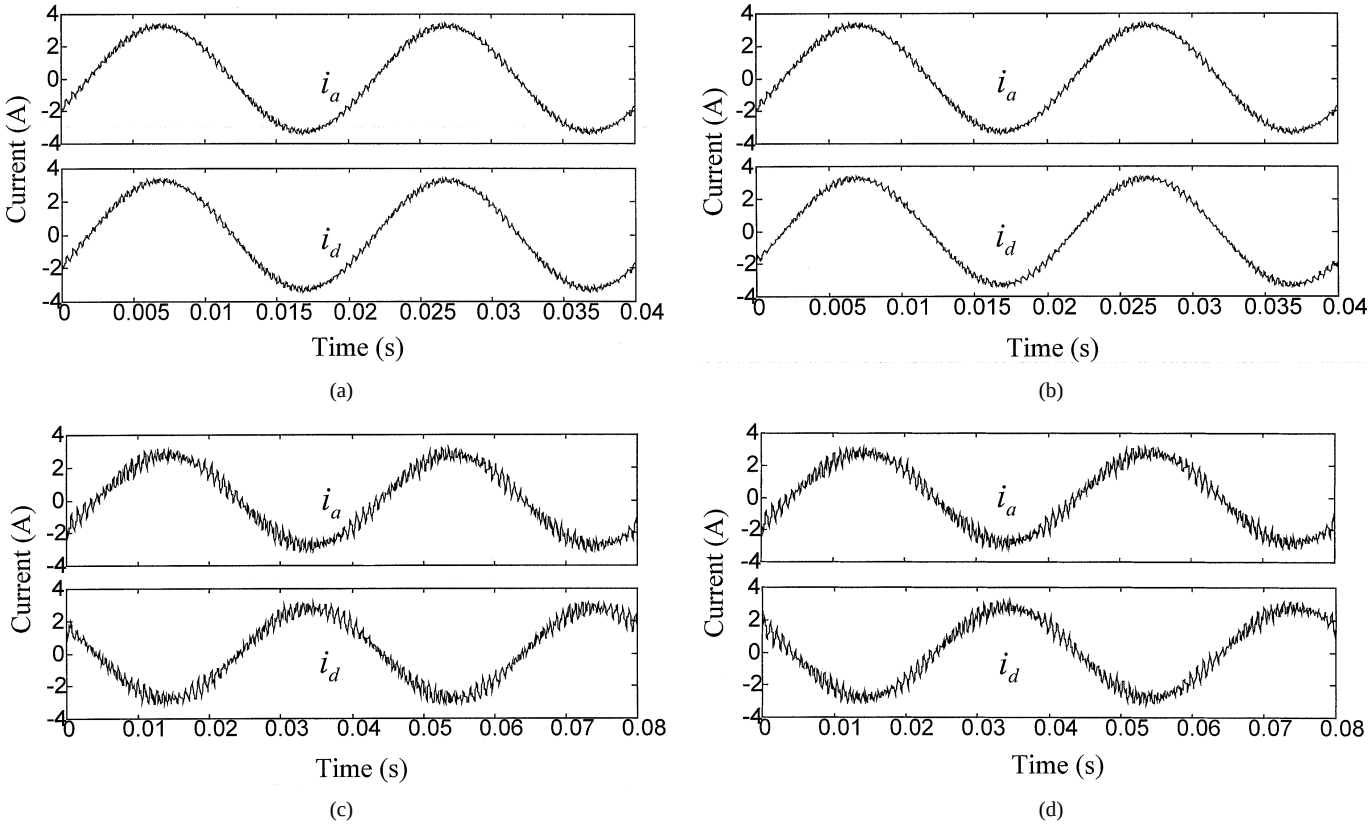

Fig. 5. Simulated current waveforms. (a) 4P1. (b) 4P2. (c) 2P1. (d) 2P2.

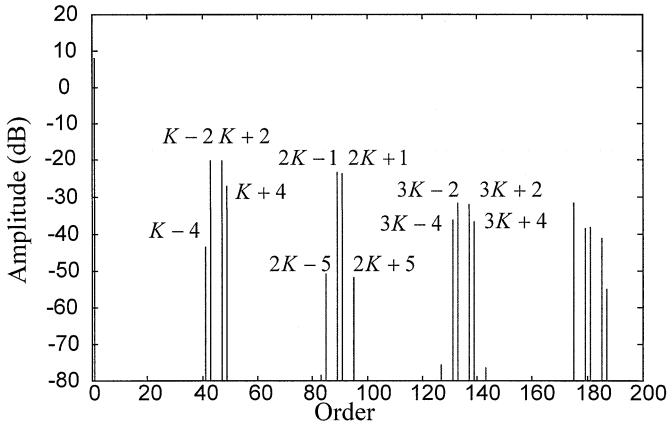

Fig. 6. Simulated spectrum of phase-a current.

$$
\begin{aligned}
i_{abc,\mathrm{odd}} =& \frac{3B_{01}}{2V_d} \sum_{\substack{i=1,3,5\\ iK+j\neq 3h}}^{\infty} \sum_{\substack{l=0,\pm1,\pm2\\ j=6l-2}}^{\pm\infty} \frac{A_{ij}}{|Z_{A,ij}|} \\
&\times \sin[i\omega_c t + (j-1)\omega_r t - \varphi_{A,ij}] \\
&- \frac{3B_{01}}{2V_d} \sum_{\substack{i=1,3,5\\ iK+j\neq 3h}}^{\infty} \sum_{\substack{l=0,\pm1,\pm2\\ j=6l-4}}^{\pm\infty} \frac{A_{ij}}{|Z_{A,ij}|} \\
&\times \sin[i\omega_c t + (j+1)\omega_r t - \varphi_{A,ij}] \\
&+ \frac{3B_{01}}{2V_d\,|Z_1|} \sum_{i=1,3,5}^{\infty} \sum_{\substack{l=0,\pm1,\pm2\\ j=6l-2}}^{\pm\infty} A_{ij} \\
&\times \sin[i\omega_c t + (j-1)\omega_r t + \varphi_1] \\
&- \frac{3B_{01}}{2V_d\,|Z_1|} \sum_{i=1,3,5}^{\infty} \sum_{\substack{l=0,\pm1,\pm2\\ j=6l-4}}^{\pm\infty} A_{ij} \\
&\times \sin[i\omega_c t + (j+1)\omega_r t - \varphi_1] \\
&+ i_{a,\mathrm{odd}}(\omega_c t, \omega_r t) + i_{a,\mathrm{odd}}\left(\omega_c t, \omega_r t - \frac{2\pi}{3}\right) \\
&+ i_{a,\mathrm{odd}}\left(\omega_c t, \omega_r t + \frac{2\pi}{3}\right) \qquad (18)
\end{aligned}
$$

where

$$
\begin{aligned}
i_{a,\mathrm{even}}(\omega_c t, \omega_r t) =& \frac{1}{V_d} \sum_{i=1,3,5}^{\infty} \sum_{j=0,\pm2,\pm4}^{\pm\infty} A_{ij} \\
&\times \cos(i\omega_c t + j\omega_r t) \\
&\cdot \sum_{\substack{m=1,3,5\\ mK+n\neq 3h}}^{\infty} \sum_{\substack{n=0,\pm2,\pm4\\ mK+n\neq iK+j}}^{\pm\infty} \frac{A_{mn}}{|Z_{A,mn}|} \\
&\times \cos(m\omega_c t + n\omega_r t - \varphi_{A,mn}) \\
&+ \frac{1}{V_d} \sum_{i=2,4,6}^{\infty} \sum_{j=\pm1,\pm3,\pm5}^{\pm\infty} B_{ij} \\
&\times \sin(i\omega_c t + j\omega_r t) \\
&\cdot \sum_{\substack{m=2,4,6\\ mK+j\neq 3h}}^{\infty} \sum_{\substack{n=\pm1,\pm3,\pm5\\ mK+j\neq iK+j}}^{\pm\infty} \frac{B_{mn}}{|Z_{B,mn}|} \\
&\times \sin(m\omega_c t + n\omega_r t - \varphi_{B,mn}) \qquad (19)
\end{aligned}
$$

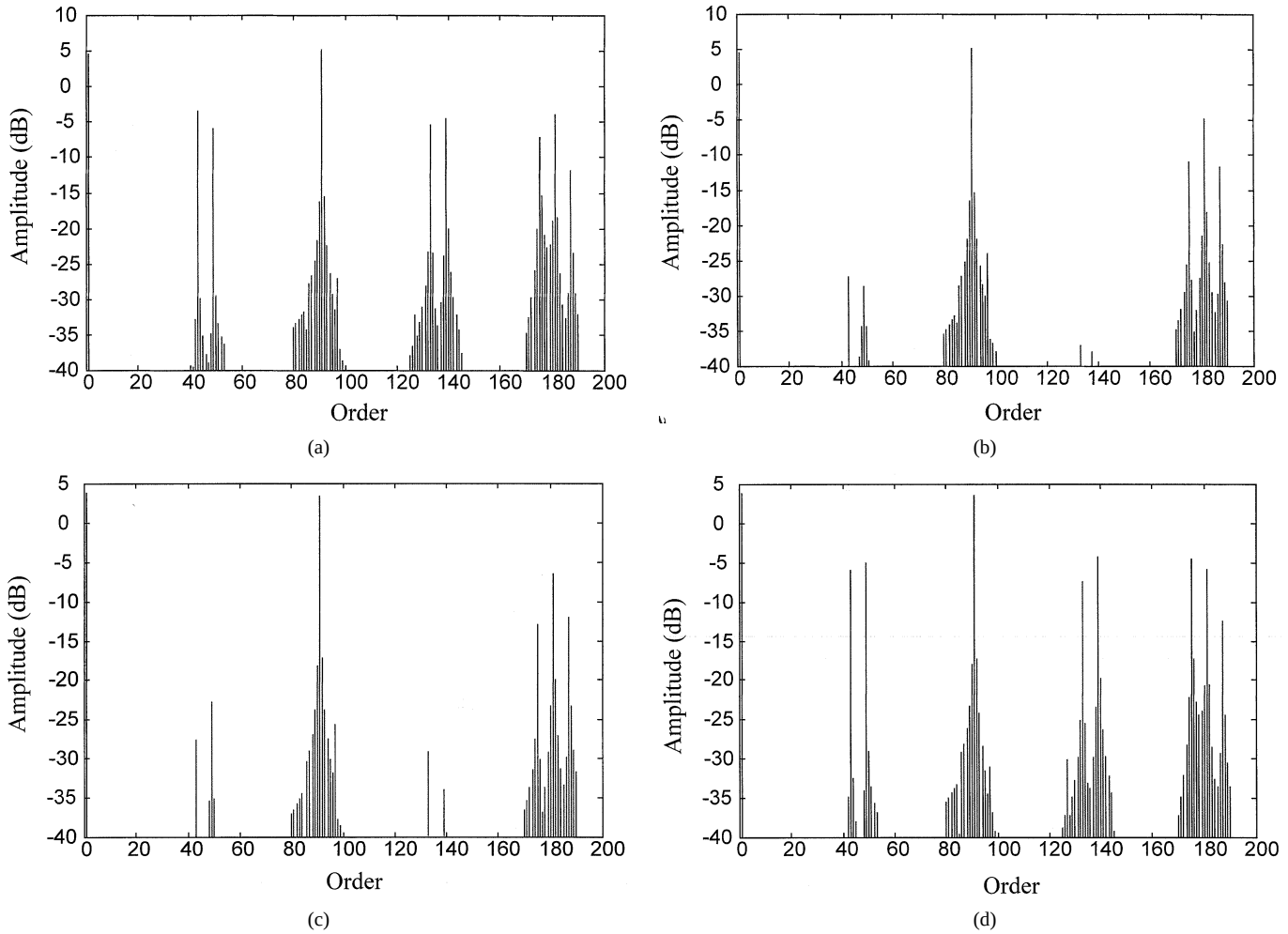

Fig. 7. Simulated current spectra of dc link. (a) 4P1. (b) 4P2. (c) 2P1. (d) 2P2.

$$
\begin{aligned}
i_{a,\mathrm{odd}}(\omega_c t,\omega_r t) =& \frac{1}{V_d}\sum_{i=1,3,5}^{\infty}\sum_{j=0,\pm2,\pm4}^{\pm\infty} A_{ij} \\
&\times \cos(i\omega_c t + j\omega_r t) \\
&\cdot \sum_{m=2,4,6}^{\infty}\sum_{\substack{n=\pm1,\pm3,\pm5\\ mK+n\neq 3h}}^{\pm\infty} \frac{B_{mn}}{|Z_{B,mn}|} \\
&\times \sin(m\omega_c t + n\omega_r t - \varphi_{B,mn}) \\
&+ \frac{1}{V_d}\sum_{i=2,4,6}^{\infty}\sum_{j=\pm1,\pm3,\pm5}^{\pm\infty} B_{ij} \\
&\times \sin(i\omega_c t + j\omega_r t) \\
&\cdot \sum_{m=1,3,5}^{\infty}\sum_{\substack{n=0,\pm2,\pm4\\ mK+j\neq 3h}}^{\pm\infty} \frac{A_{mn}}{|Z_{A,mn}|} \\
&\times \cos(m\omega_c t + n\omega_r t - \varphi_{A,mn}). \quad (20)
\end{aligned}
$$

Notice that the components in (16) are dc currents, and are generated by the same order of voltages and currents. The components in (17) are even harmonic currents centered on the even multiples of the carrier frequency. The order number of the harmonics in the first four terms is $mK \pm 6n$ where m is even. From (19), it can be found that the amplitudes of the harmonic currents in the last three terms in (17) are much smaller than

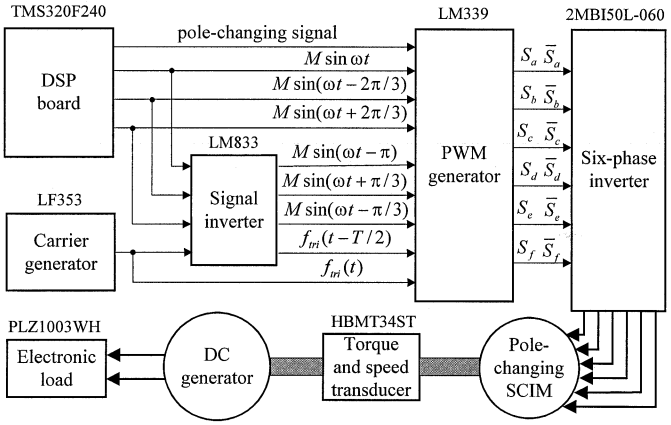

Fig. 8. Hardware implementation setup.

that of the harmonic currents in the first four terms. The components in (18) are still even harmonic currents, but they center on the odd multiples of the carrier frequency. The order number of the harmonics in the first four terms is $mK \pm 3(2n-1)$ where m is odd. From (20), the amplitudes of the harmonics in the last three terms in (20) are also much smaller than that of the harmonics in the first four terms. Hence, if only odd harmonic currents exist in the phase currents, the even harmonic currents will be exclusively present in the dc link. Moreover, they center

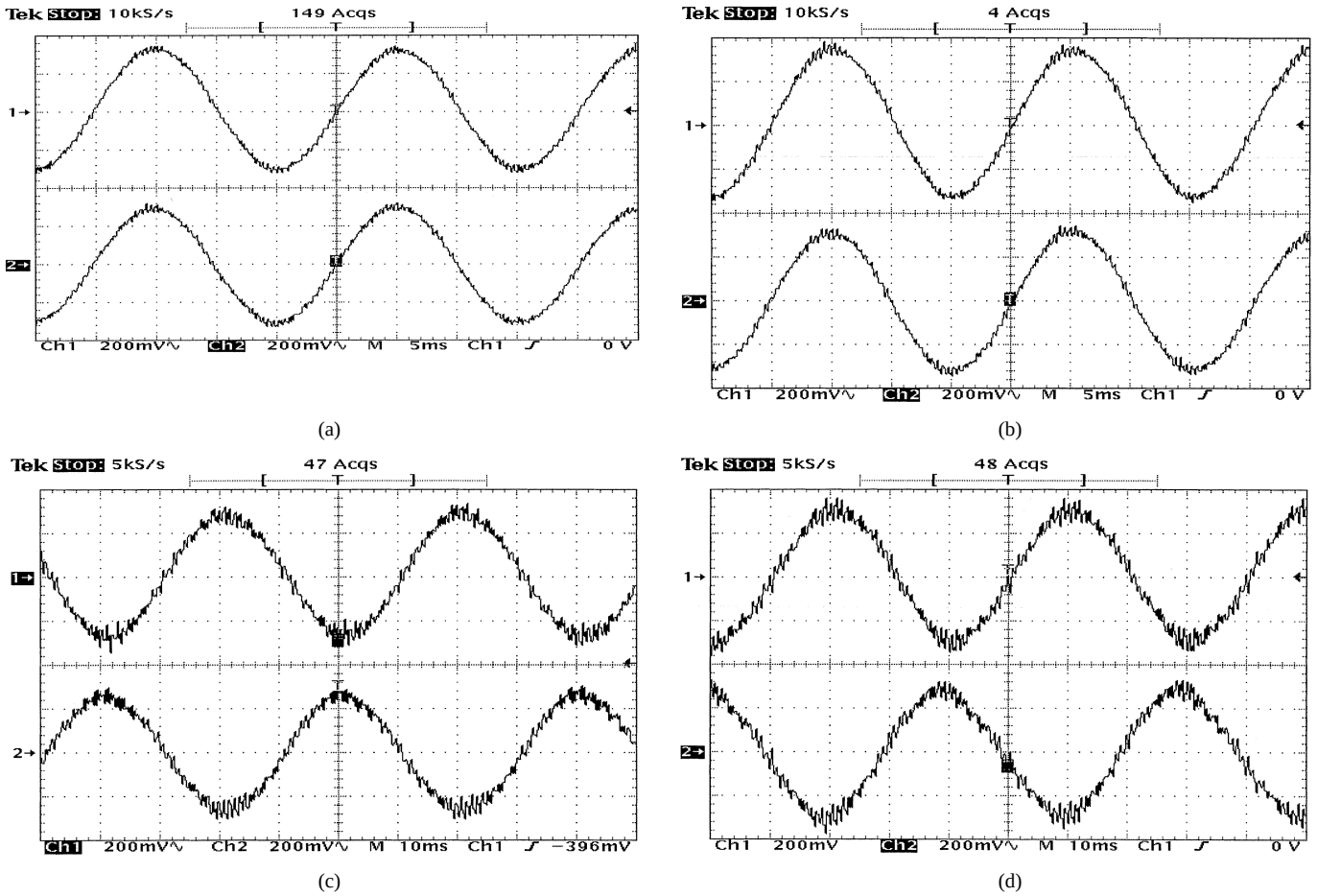

Fig. 9. Measured current waveforms (upper trace: phase a; lower trace: phase d; 2 A/div, 5 ms/div). (a) 4P1. (b) 4P2. (c) 2P1. (d) 2P2.

on the multiples of the carrier frequency, and the amplitudes of even triplen harmonics are larger than that of other harmonics.

Similar to (15), the second part in (14) can also be expressed as

$$\frac{u_d i_d + u_e i_e + u_f i_f}{V_d} = i_{\text{def,DC}} + i_{\text{def,even}} + i_{\text{def,odd}}. \quad (21)$$

By comparing the double Fourier series coefficients for the cases 4P1 and 4P2 in Table I, the following is determined:

$$i_{\text{def,DC}} = i_{abc,\text{DC}} \quad (22)$$

$$i_{\text{def,even}} = i_{abc,\text{even}}. \quad (23)$$

For the case 4P1, the last terms in (15) and (21) are governed by

$$i_{\text{def,odd}} = i_{abc,\text{even}}. \quad (24)$$

On the contrary, for the case 4P2, they are governed by

$$i_{\text{def,odd}} = -i_{abc,\text{even}}. \quad (25)$$

By substituting (22)–(24) into (14), the dc-link current in the case 4P1 can be obtained as

$$i = 2(i_{abc,\text{DC}} + i_{abc,\text{even}} + i_{abc,\text{odd}}). \quad (26)$$

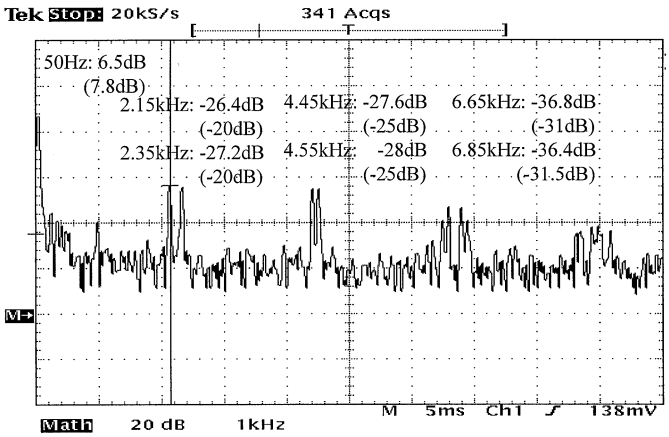

Fig. 10. Measured spectrum of phase-a current.

Similarly, by substituting (22), (23), and (25) into (14), the dc-link current in the case 4P2 is obtained as

$$i = 2(i_{abc,\text{DC}} + i_{abc,\text{even}}). \quad (27)$$

A comparison of (26) and (27) shows that the case 4P2 takes a definite advantage over the case 4P1 that the harmonic centered on the odd multiples of carrier frequency is eliminated. The derivation of (26) and (27) is also applicable for two-pole operation, respectively, the cases 2P2 and 2P1, but with different

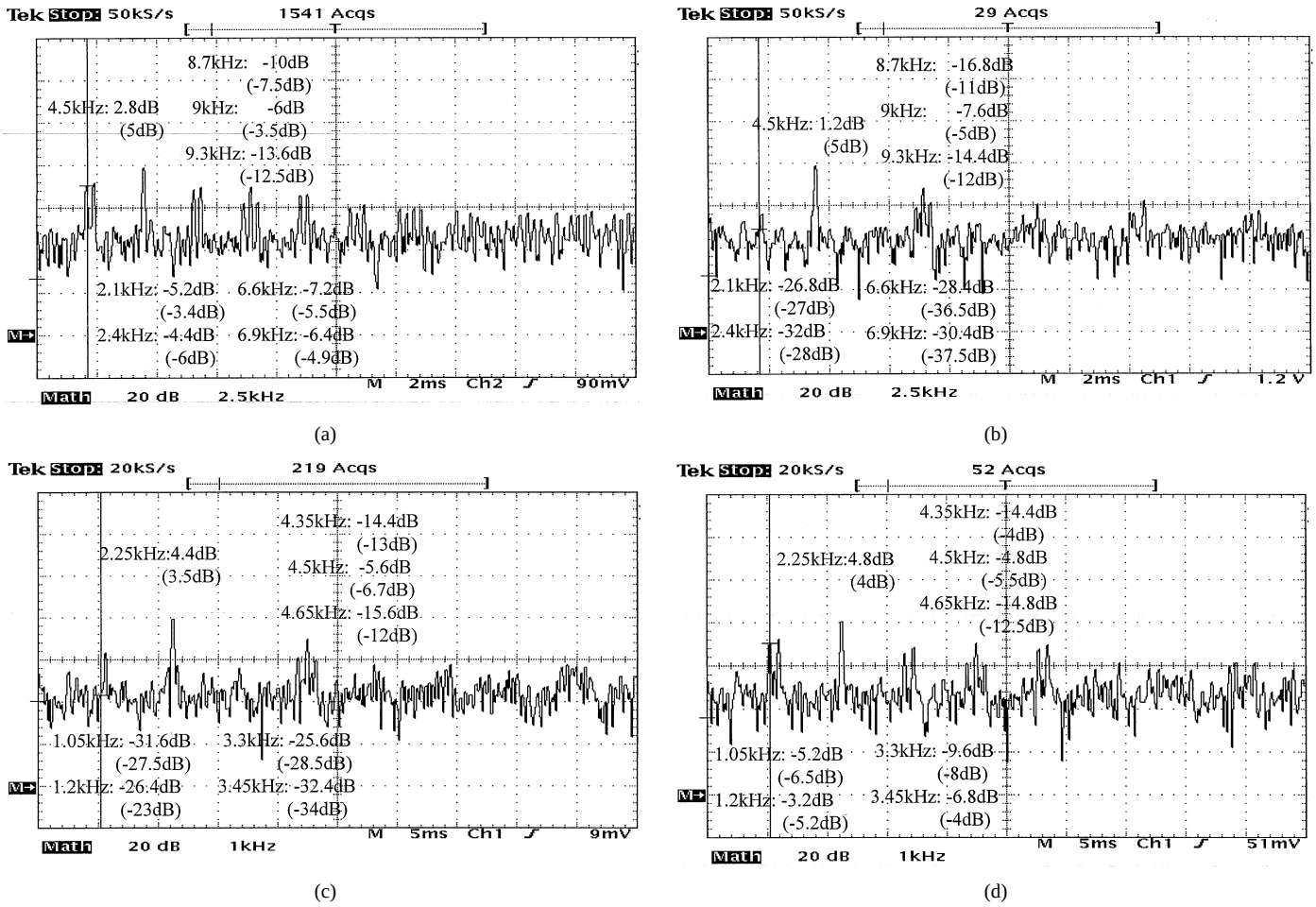

Fig. 11. Measured current spectra of dc link. (a) 4P1. (b) 4P2. (c) 2P1. (d) 2P2.

coefficients in (16)–(18). These coefficients are decided by the equivalent input impedances and the double Fourier series coefficients. Under the same conditions, the spectra of the dc-link currents for the four possible cases are shown in Fig. 7. It can be observed that the harmonic contents centered on the odd multiples of the carrier frequency in the cases 4P2 and 2P1 are significantly lower than those in the cases 4P1 and 2P2, respectively. Therefore, 4P2 and 2P1 are respectively superior to 4P1 and 2P2 for the proposed six-phase pole-changing SCIM drive.

V. Experimental Results

In order to verify the spectral analysis of the proposed six-phase pole-changing SCIM drive, the system is prototyped and tested. Fig. 8 shows a block diagram of the test system, in which the digital signal processor (DSP) TMS320F240 board is adopted to produce the sinusoidal references. Notice that this DSP board will also be used to implement a sophisticated control algorithm in a later stage. The frequency of the triangular carrier is selected to keep the modulation ratio equal to 45. Then, the sinusoidal PWM switching signals for the insulated-gate-bipolar-transistor (IGBT)-based six-phase inverter are generated by the PWM generator. The experimental six-phase pole-changing SCIM is 0.7 kW, and can electronically switch between four and two poles.

For the cases 4P1 and 4P2, the frequencies of the reference signals are selected at 50 Hz; whereas, for the cases 2P1 and 2P2, the reference signals are selected at 25 Hz. Therefore, the synchronous speed of the SCIM in all four cases is kept at 1500 r/min. The carrier frequency used in the cases 4P1 and 4P2 is 2250 Hz and that in the cases 2P1 and 2P2 it is 1125 Hz. The measured phase current waveforms, for 4P1 and 4P2 as well as 2P1 and 2P2, at the load of 150 W are shown in Fig. 9. The spectrum of phase a current in the case 4P1 is shown in Fig. 10, in which the bracketed values are the corresponding simulated results. It can be seen that these experimental results agree well with the simulation results shown in Figs. 5 and 6. The measured spectra of the harmonic currents in the dc link are shown in Fig. 11, where the simulated results are also listed with brackets for direct comparisons. It can be observed that the case 4P2 takes the advantage over the case 4P1 that the harmonic amplitudes centered on the odd multiples of the carrier frequency are greatly suppressed. Similarly, the spectrum of the case 2P1 has such a harmonic suppression. Therefore, both experimental and simulated results confirm that 4P2 is preferred to 4P1 for four-pole operation, while 2P1 is preferred to 2P2 for two-pole operation.

VI. Conclusion

A new six-phase pole-changing SCIM drive has been presented, which is particularly suitable to extend the constant-

power operating range for EVs. The key is to propose a new sinusoidal PWM strategy in such a way that the two carriers of the six-phase inverter are out of phase during four-pole operation, whereas they are in phase during two-pole operation. With the use of double Fourier series, both the phase currents and, hence, the dc-link current have been analytically derived, indicating that the dc-link harmonics centered on the odd multiples of the carrier frequency can be eliminated. Experimental results have been given to support the theoretical spectral analysis.

With the use of the proposed PWM strategy, the dc-link harmonic currents can be significantly reduced, hence, improving the battery lifetime which dominates the operating cost of EVs. Although the proposed PWM strategy has adopted the sinusoidal PWM scheme, it can readily be extended to other schemes such as space-vector PWM and optimized PWM.

ACKNOWLEDGMENT

The authors would like to thank Prof. Z. Q. Zhu for his valuable information.

REFERENCES

[1] C. C. Chan and K. T. Chau, "An overview of power electronics in electric vehicles," *IEEE Trans. Ind. Electron.*, vol. 44, pp. 3–13, Feb. 1997.

[2] M. Mori, T. Mizuno, T. Ashikaga, and I. Matsuda, "A control method of an inverter-fed six-phase pole change induction motor for electric vehicles," in *Proc. Int. Power Conversion Conf.*, Nagaoka, Japan, 1997, pp. 25–32.

[3] S. Z. Jiang, K. T. Chau, and C. C. Chan, "Performance analysis of a new dual-inverter pole-changing induction motor drive for electric vehicles," *Elect. Mach. Power Syst.*, vol. 30, no. 1, pp. 11–29, Jan. 2002.

[4] K. T. Chau, Y. S. Wong, and C. C. Chan, "An overview of energy sources for electric vehicles," *Energy Convers. Manage.*, vol. 40, no. 10, pp. 2021–2039, July 1999.

[5] J. Holtz, "Pulsewidth modulation for electronic power conversion," *Proc. IEEE*, vol. 82, pp. 1194–1214, Aug. 1994.

[6] V. Weisgerber, "Double-pulse inverter feeds 6-phase asynchronous motor for harmonic loss reduction," in *Proc. Eur. Conf. Power Electronics and Applications*, 1993, pp. 39–44.

[7] J. Shen, J. A. Taufiq, and A. D. Mansell, "Analytical solution to harmonic characteristics of traction PWM converters," *Proc. IEE —Elect. Power Applicat.*, vol. 144, no. 2, pp. 158–168, Mar. 1997.

S. Z. Jiang was born in China in 1967. He received the B.S. and M.S. degrees in electrical engineering from Harbin Institute of Technology, Harbin, China, in 1989 and 1992, respectively. He is currently working toward the Ph.D. degree in the Department of Electrical and Electronic Engineering, University of Hong Kong, Hong Kong.

From 1992 to 1998, he was with the Department of Electrical Engineering, Shanghai Jiao Tong University, Shanghai, China. His current research interests are in the optimum control of PWM inverters, analysis and control of electrical machines, and microcontroller-based systems.

K. T. Chau (M'89) received his first-class honors B.Sc.(Eng.), M.Phil., and Ph.D. degrees in electrical and electronic engineering from The University of Hong Kong, Hong Kong.

He is currently an Associate Professor at The University of Hong Kong. His teaching and research interests focus on three main areas: power converters, machines and drives, and electric vehicles. In these areas, he has authored more than 100 published refereed technical papers and several industrial reports. He has also served as chair and organizing committee member for many international conferences. He is the coauthor of a monograph, *Modern Electric Vehicle Technology* (London, U.K.: Oxford Univ. Press, 2001).

C. C. Chan (M'77–SM'77–F'92) received the B.Sc. degree from China University of Mining and Technology, Beijing, China, the M.Sc. degree from Tsinghua University, Beijing, China, and the Ph.D. degree from The University of Hong Kong, Hong Kong, in 1953, 1957, and 1981, respectively.

He is currently Chair Professor in the Department of Electrical and Electronic Engineering, The University of Hong Kong. He has authored four books and more than 120 published technical papers and is the holder of seven patents.

Prof. Chan is a Fellow of the Royal Academy of Engineering, U.K., an Academician of the Chinese Academy of Engineering, and a Fellow of the Ukraine Academy of Engineering Science. He was awarded the Honorary D.Sc. degree from the University of Odessa in 1992.